Exploring Ion Suppression in Mass Spectrometry Imaging of a Heterogeneous Tissue

Adam J Taylor (1)
Alex Dexter (1)
Josephine Bunch* (1,2)

1. National Centre of Excellence in Mass Spectrometry Imaging (NiCE-MSI), National Physical Laboratory, Hampton Road, Teddington, TW11 0LW, UK

2. Department of Surgery and Cancer, Imperial College London, South Kensington Campus, London, SW7 2AZ, UK

* Corresponding author. Email: josephine.bunch@npl.co.uk

Abstract

In this study we have explored several aspects of regional analyte suppression in mass spectrometry imaging of a heterogeneous sample; transverse cryosections of mouse brain. Olanzapine was homogeneously coated across the section prior to DESI and MALDI mass spectrometry imaging. We employed the concept of a tissue extinction coefficient (TEC) to assess suppression of an analyte on tissue relative to its intensity in an off tissue region. We expanded the use of TEC, by first segmenting anatomical regions using graph-cuts clustering, and calculating a TEC for each cluster. The single ion image of the olanzapine $[M+H]^+$ ion was seen to vary considerably across the image, with anatomical features such as the white matter and hippocampus visible. While trends in regional ion suppression were conserved across MSI modalities, significant changes in the magnitude of relative regional suppression effects between techniques were seen. Notably the intensity of olanzapine was less suppressed in DESI than for MALDI. In MALDI MSI, significant differences in the concentration dependence of regional TECs were seen, with the TEC of white matter clusters exhibiting a notably stronger correlation with concentration than for clusters associated with grey matter regions. We further employed cluster-specific TECs as regional normalisation factors. In comparison to published pixel-by-pixel normalisation methods, regional TEC normalisation exhibited superior reduction ion suppression artefacts. We also considered the usefulness of a segmentation-based approach to compare spectral information obtained from complementary modalities.

Introduction

Many different modalities of mass spectrometry imaging (MSI) have been implemented and applied to the analysis of biological samples. Their diverse methods of desorption and ionisation of analytes from the sample facilitate the detection of many different classes of analyte including small molecule drugs and metabolites, lipids and small peptides. All modalities of MSI assume a semi-quantitative relationship between amount of substance and detected ion intensity. Therefore, an understanding of variations in the efficiency of extraction, desorption, ionisation and detection of analytes is essential in interpreting MSI data. The maturation and wider adoption of mass spectrometry imaging is enabling the analysis of biological samples of great spatial, chemical and structural heterogeneity. As the chemical composition and structural properties of the sample vary pixel-by-pixel, aspects of ion suppression and enhancement can drastically alter the relative contrast and information obtained from the resulting MS image.

Ion suppression is complicated and is the result of many competing factors. The influence of the diverse molecular components of the sample can have on the extraction, desorption and ionisation of a chosen analyte of interest are collectively described as the matrix effect[1]. Beyond the matrix effect, other influencers of detected ion yield will include physical properties of the sample[2] and substrate[3], as well as ionisation method variables such MALDI matrix crystal properties, laser fluence and repetition rate[4–6].

Ion suppression has been considered for a range of analyte classes, although small molecule drugs and endogenous lipids have been most commonly discussed. Ion suppression effects are widespread and will impact, to greater or lesser extent, all mass spectrometry modalities. They have been considered for all main mass spectrometry imaging modalities including MALDI[7–9],DESI[10], secondary ion mass spectrometry (SIMS)[11–15], nanoDESI[16] and laser ablation inductively coupled plasma mass spectrometry (LA ICP MS)[17], as well as for other spatially resolved techniques such as liquid extraction surface analysis mass spectrometry (LESA)[18] and laser microdissection-liquid vortex capture-mass spectrometry [19]. For some techniques, particularly SIMS, ion suppression and matrix effects have been considered extensively from a metrology perspective[11], while in other modalities discussion of ion suppression and the resulting effects on ion intensity have been more often considered in the context of assessing normalisation strategies[16,20].

There are several reasons why an understanding of, and correction for, matrix effects is important for MSI of biological samples. Firstly, differing analyte suppression across a sample may lead to false apparent spatial distributions[21]. This is particularly important in heterogeneous tissues where diverse biological and structural environments may induce strong changes in relative ion suppression between anatomical regions. For example, Lanekoff *et al*. incorporated two endogenous lipid internal standards into the solvent in a nanoDESI experiment[16]. Normalisation to these internal standards revealed and enabled control of differential suppression of lipid ion yield seen between ischemic and healthy regions of brain tissue. A similar approach later enabled quantitation of small molecule neurotransmitters by nanoDESI[21]. Matrix effects may also drive the ionisation of species towards or away from a particular polarity or adduct form[16]. The impact of adduct form will be particularly acute when selecting precursor ions for MS/MS imaging experiments[22,23].

Matrix effects may additionally hinder approaches for both relative and absolute quantitation. Normalization is a widely used pre-processing step in many data analysis workflows for mass spectrometry imaging data. Normalisation approaches can be categorized as scan-by-scan spectral normalisation, normalization to an internal standard, and region-specific normalisation approaches. In MSI pixel-wise normalisation of ion intensities using a total ion intensity (TIC) scaling factor is most often reported. However, Deininger *et al*. showed that in many cases normalisation on the median and the noise level was more robust against artefact generation compared to normalisation on the TIC[20]. Recently, these non-TIC approaches for normalisation have been implemented in software for the analysis of MSI data[24], and other normalisation methods have been explored and implemented [9].

The use of internal standards for normalisation has become commonplace in mass spectrometry imaging workflows where absolute quantitation is required, and has been implemented in software for analysis of MSI data [25]. Källback *et al.* showed that normalisation to a homogeneously distributed internal standard yielded greater linearity of calibration curves of spotted standards than other normalisation methods[26]. However, appropriate internal standards may not always be available. Ideal internal standards are (1) structurally identical with appropriate isotopic labelling to shift the observed mass-to-charge ratio away from the observed isotope pattern of the unlabelled compound; (2) are stable, available and affordable; (3) are influenced by matrix effects to the same degree as the unlabelled compound. Appropriate selection and placement of internals standards and of calibration standards is also important, particularly for heterogeneous tissues and comparison between organs.

Organs can present various diverse biological environments which may therefore induce differing levels of ion suppression. This has been demonstrated and discussed in a number of studies including MSI of whole-body sections[27], excised organs[28] and tissue homogenates prepared from different organs[29]. Hamm *et al*. examined these effects in different whole organs in MALDI MSI of mouse whole body sections [7]. The authors proposed a "tissue extinction coefficient" (TEC) as a scaling factor, calculated by comparing the mean intensity of a standard on the tissue and on the bare substrate. By manual selection of regions of interest the relative level of ion suppression between organs could be compared. As this approach considers regions of interest rather than working pixel-by-pixel, it appears useful both to reveal regions that induce higher or lower levels of analyte suppression and to compare suppression between mass spectrometry imaging modalities. The majority of the studies described above considered single mass spectrometry imaging techniques, as multimodal studies become more prevalent, it is important to consider the relative suppression effects seen not only between regions, but also between ionisation methods.

As the achievable spatial resolution of mass spectrometry imaging modalities techniques has increased, it has become possible to resolve finer features of anatomy within heterogeneous tissues such as brain[30]. In many samples, anatomy and pathology may not be conserved between sections, treatment groups or biological replicates, hindering the ability to manually annotate regions of interest. There is therefore a need for unsupervised methods to select anatomical regions that are small and difficult to outline or for which an anatomical atlas is not available. Advances in clustering algorithms such as graph cuts now facilitate unbiased segmentation of anatomical regions from mass spectrometry imaging datasets[31,32].

Here we studied regional ion suppression of a model small molecule analyte, the antipsychotic drug olanzapine, in MALDI and DESI imaging of transverse cryosections of mouse brain. Homogeneous deposition of olanzapine across the highly heterogeneous brain anatomy provided a useful model system. Specifically we addressed the following aims. Firstly we set out to use graph cuts segmentation to identify regions of high and low suppression of olanzapine in DESI and MALDI MSI of transverse mouse brain. Secondly we compared regional analyte suppression effects in the same model system between DESI and MALDI MSI. Thirdly we assessed the concentration dependence of regional analyte suppression effects. Additionally we compared a segmentation-based TEC normalisation method to

other published normalisation techniques. Finally we looked at the potential of these approaches to compare spectral information obtained from complementary mass spectrometry imaging ionisation methods.

Experimental Section

Tissue preparation

Whole wild-type mouse brains were snap frozen in liquid nitrogen after post-mortem excision and stored at -80°C until use. Cryosections were taken -20°C in the transverse (horizontal) plane at 10 µm thickness on a cryostat (CM1850, Leica, Milton Keynes, UK), and thaw-mounted onto glass slides (SuperFrost Plus™, Thermo Scientific, Waltham, MA, USA) . Sections were stored at -80°C until analysis. On removal from storage at -80°C, sections were immediately transferred to a vacuum desiccator for approximately 20 minutes until condensation was removed.

Olanzapine deposition

Olanzapine (O1141, Sigma-Aldrich,Gillingham, UK) was homogeneously deposited by sublimation or automated spraying. Sublimation was performed using an Edwards Auto 306 vacuum coater (Edwards, Burgess Hill, UK). 10 mg of olanzapine was placed in a molybdenum boat with a labyrinthine exit (ME1, Testbourne, Basingstoke, UK). A vacuum was applied to the chamber and voltage across the boat gradually increased until sublimation commenced. Deposition rate and thickness was monitored using quartz crystal microbalance set at the same distance from the boat as the sample. A density of 1.1 g/cm^3 was assumed for rate and thickness monitoring. The deposition rate was maintained below 10 nm/s. Sublimation was stopped at 1 µm calculated thickness. This represents an estimated density of Olanzapine per unit area of 4.16 nmol/mm^2, assuming an Olanzapine density of 1.3 g/cm^3. Spraying of olanzapine was performed using an automated pneumatic sprayer (TM-sprayer, HTX imaging, Chapel Hill, NC, USA). Olanzapine, at concentrations of 0.1, 0.5 or 1 mg/ml in 80:20 (v:v) methanol-water, was delivered at 0.06 µl/min by an isocratic HPLC pump (40P, Knauer, Berlin, Germany) through a nebulising head heated to 65°C. The nebulising gas was nitrogen delivered at 15 mbar. The spray head was rastered at 1333 mm/min in a sawtooth pattern with a track spacing of 3 mm across the microscope slide for 16 passes, alternating raster direction for each pass. Resulting Olanzapine area densities were

estimated as 77, 384 and 768 pmol/mm^2 respectively. A blank was prepared by spraying 80:20 (v:v) methanol-water only using the same protocols.

Mass spectrometry imaging

MALDI sample preparation

Immediately prior to analysis, α-Cyano-4-hydroxycinnamic acid (CHCA) was deposited at 6.35 nmol/mm^2 using an automated pneumatic sprayer (TM-sprayer, HTX imaging, Chapel Hill, NC, USA). 5 mg/ml CHCA (476870, Sigma-Aldrich, Gillingham, UK) in 80:20 (v:v) methanol-water was deposited using the same deposition parameters as for Olanzapine spraying described above.

MALDI MSI

MALDI MSI was performed on a Synapt G2-Si MALDI mass spectrometer (Waters, Milford, MA, USA), operated in positive ion polarity across a mass range of m/z 100-1200. The instrument was operated in resolution mode (single-pass reflectron ToF). Prior to analysis the instrument was mass calibrated using red phosphorus spotted onto a steel plate. An Nd:YAG laser (355 nm) was used with a repetition rate of 2500 Hz and a mean laser energy per pulse of 4 µJ (software setting of 250 arbitrary units).. The resulting laser spot size was approximately 60 µm in diameter. Scan time was set at 0.1 s, Pixel size was set at 45 µm in both the *x* and *y* axis.

DESI MSI

DESI MSI was performed using a Waters/Prosolia DESI source attached to a Waters Synapt G2-Si Q-IMS-oaToF mass spectrometer (Waters, Milford, MA, USA). The electrospray solvent was 95:5 (v:v) methanol:water, supplemented with 0.01 mg/ml raffinose as an referencecompound used for subsequent recalibration of the mass axis. Solvent was delivered at 2 µl/min using a 2.5 ml Hamilton syringe and a Legato 100 syringe pump. The electrospray voltage was 5 keV. The resulting DESI spot size was approximately 500 µm in diameter as measured by ablation of rhodamine sublimated on a glass slide. The instrument was operated in positive ion polarity, in “resolution” mode (single reflectron ToF), and was mass calibrated prior to acquisition using the MS/MS of [Glu1]-Fibrinopeptide B (700004729, Waters, Milford, MA, USA) across a mass range of m/z 100-1200 with a trap collision energy of 35 V. A nominal pixel size of 50 µm was set in both *x* and *y* axis using a stage raster speed of 100 µm/s and a scan time of 0.485 s with a 0.015 s interscan delay.

Data analysis

Data were converted from Waters' RAW format to the standardised, open access imzML format[33] using imzML converter[34]. Data were analysed in MATLAB (versions 2014b to 2017a, MathWorks, Natick, MA, USA), SpectralAnalysis (versions 1.00 to 1.1)[24], R (version 3.4.0, R Foundation, Vienna, Austria)[35] and RStudio (version 1.0.143, RStudio, Boston, MA, USA). The workflow for clustering, TEC calculation and normalisation is shown in figure 1. As colourmap selection can alter contrast perception[36], all ion images are displayed using the perceptually uniform *Viridis* colourmap[37,38]. Initially a mean spectra was generated for *m/z* 400-1200. Peaks below m/z 400, were removed to eliminate the influence of expected adducts and fragments of olanzapine on subsequent clustering, therefore removing suppression bias. Mean spectra were peak picked using a gradient method and and the top 2000 intense peaks selected for further analysis. The mass axis of the DESI datasets were recalibrated using accurate mass of the lockmass compound, raffinose, and known abundant lipids. Tissue was segmented from background by *k*-means clustering with cosine distance and k=2[31]. Graph cuts clustering[32] of the tissue region was performed in MATLAB. Five replicate segmentation runs were performed. While all replicates were assessed to confirm reproducibility of segmentation, only the first replicate was used for further analysis and visualisation. Segmented data were further analysed in R and RStudio. TECs for each cluster were calculated by dividing the mean intensity of the olanzapine $[M+H]^+$ peak in the cluster region by the intensity of the same peak in the off-tissue, background region. Previously published normalisation methods were applied as implemented in SpectralAnalysis using the peak-picked data across the full mass range. Using each matched cluster as a mask, peaks picked from mean spectra across the whole acquired mass range (m/z 100-1200) were matched to the HMDB database[39–41] using custom MATLAB scripts. Results were filtered to select assignments with <10 ppm mass deviation and a similarity of R^2 >= 0.5 between the image of the monoisotopic assignment and the ^{13}C isotope image.

Results and discussion

Regional suppression

Results were used to assess analyte suppression in different regions of a model heterogeneous tissue, mouse brain, with two of the most widely reported mass spectrometry imaging techniques, DESI and MALDI MSI.

Single ion images of m/z 313.15, olanzapine $[M+H]^+$, from analysis by DESI and MALDI MSI are shown in figure 2A. Although the analyte was deposited homogeneously across the sample, significant variance in the intensity of the intact $[M+H]^+$ molecular ion are observed across the tissue for both techniques. From observation, the spatial distribution of intensity appears to correlate closely with the expected anatomy of the tissue, partially distinguishing the grey and white matter. This is particularly noticeable in the MALDI MSI image. Clearly, different regions of anatomy within the tissue section are influencing analyte extraction, desorption and ionisation of the nominally heterogeneous analyte. Here we collectively describe these as ion suppression effects. Additionally some differences between DESI and MALDI are obvious from the single ion image of olanzapine. In DESI the delineation between grey and white matter in the olanzapine image is less stark than for MALDI MSI, and the range of analyte intensities is reduced.

To explore these effects further we set out to define expected anatomical regions seen in both DESI and MALDI MSI datasets. “Graph cuts clustering is a spatial segmentation algorithm that uses the spectral similarity of pixels to create a connectivity graph, and then partitions this graph aiming to preserve as much connectivity as possible.“ The graph cuts algorithm has been demonstrated to yeild visibly clearer segmentation of expected anatomical regions than other clustering algorithms when applied to an MS image from coronal mouse brain, with excellent correlation between segmented regions and anatomical regions defined in the Allen Mouse Brain Atlas [32]. After segmenting tissue from background by *k*-means clustering with k=2 and cosine distance [31], we separately applied graph cuts clustering with k=15 to peaks selected from the m/z 400-1200 mass range of the tissue region of the DESI and MALDI MSI datasets. This reduced mass range was selected to reduce the influence of the olanzapine by removing the mass range below m/z 400 were expected adducts and fragments might lie. Clustering across this

restricted mass range was not found to substantially alter segmentation of expected anatomy compared to removing a black-list of peaks found in the off tissue region (Figure S-1).

From manual inspection of the clustering images, four matching clusters from DESI and MALDI data were selected manually and identified with reference to an annotated horizontal mouse brain atlas of magnetic resonance imaging (MRI) data[42]. These selected clusters are shown in figure 2B and can be labelled with four major anatomical regions: the white matter (purple), the hippocampus (blue), and the granular (green) and molecular (red) layers of the cerebellum. Although sections used for both techniques are obtained from slightly different depths in the horizontal plane, these major anatomical regions were well conserved in both DESI and MALDI datasets as seen in figure 2B.

To assess the level of suppression seen in different techniques and regions, regions of interest were created for the clusters defined by the graph cuts algorithms. Boxplots showing the intensity of the olanzapine $[M+H]^+$ peak for pixels within the four selected matched clusters are shown shown in Figure 2C. Notable differences can be observed across both region and technique. Significant differences in intensity are seen between selected clusters in DESI MSI (ANOVA $Pr(>F) < 0.001$). Post-hoc testing shows that intensity white matter is significantly higher than all other selected clusters (Tukey HSD, $p<0.001$) and that intensity in the hippocampus is significantly lower than all other clusters (Tukey HSD, $p<0.001$). Intensities in the molecular and granular layers of the cerebellum were also found to be significantly different (Tukey HSD, $p<0.001$). In MALDI, as with DESI, the intensity in the white matter is significantly higher than in the other selected clusters (ANOVA $Pr(>F) <0.001$ and Tukey HSD, $p <0.001$). Differences in intensity between the other clusters are not significant (Tukey HSD, $p>0.1$), however their medians follow the same order seen in DESI, notably the hippocampus exhibiting the lowest median intensity. The spread of pixel intensities, assessed by the interquartile range, is comparable for each selected region in DESI, while in the MALDI dataset the interquartile range of the white matter region is notably larger than for the three other selected clusters.

The tissue extinction coefficient of a region can be defined as the mean intensity of a peak in a region of interest divided by the mean intensity of the same peak from the off-tissue region [7]. Here we use TEC as a useful metric to compare the relative level of analyte suppression seen between both regions and techniques, rather than directly comparing peak intensities. In this study ion intensities seen in DESI and MALDI data are not directly comparable, particularly as different MS scan times were used (0.485 s for

DESI, 0.1 s for MALDI). A TEC value lower than one indicates ion suppression of the olanzapine $[M+H]^+$ peak relative to the off-tissue region, while a TEC greater than one would indicate relative ion enhancement. Figure 2D shows TECs calculated from the selected clusters. These are additionally summarised in table 1. For each of the selected regions, TECs are more than four times higher in DESI than for MALDI, indicating DESI results in less relative ion suppression than for MALDI across a range of anatomies. None of the regions have a TEC less than 0.75 for DESI while all TECs for MALDI are below 0.25. A five-fold decrease in TEC is seen for MALDI compared to DESI for the white matter region, while the difference is even larger for the other selected regions - with MALDI TECs more than twenty times lower than their matched regions in DESI. For MALDI, the mean TEC of all clusters (0.06) is comparable to the olanzapine TEC in brain (0.07) described by Hamm *et al*. [7]

The large difference in TECs across techniques will be influenced by the relative yields from the off tissue region, as the denominator of TEC is the off tissue intensity. The desorption-ionisation techniques considered here employ greatly differing mechanisms of analyte extraction, desorption and ionisation. When the MALDI matrix is deposited using a solvent carrier, as in the TM Sprayer, an analyte deposited on glass will come into intimate contact with matrix, leading to a very high ion intensity. In DESI an analyte deposited on glass may be easily delocalised by the focussed solvent and gas flow. Delocalisation may be more limited on tissue.

For both techniques the highest TECs are seen for the white matter cluster, indicating that it exhibits the least relative ion suppression across techniques. Interestingly, a slight relative enhancement effect (TEC of 1.027) is observed for the white matter cluster in DESI.

Normalisation by cluster specific TEC

When first proposed by Hamm *et al*. the tissue extinction coefficient was proposed as a normalisation method to facilitate comparison between organs inducing differing levels of ion suppression[7]. The cluster-specific tissue extinction coefficients described in this paper may be applied as cluster-specific normalisation factors. When the normalisation factor is specific to the segmented region in which that pixel is found, this has the advantage of taking into account the spectral variance that may be seen pixel-to-pixel and provides a normalisation factor reflective of ion suppression seen across other spectrally similar pixels.

In figure 2E the intensity of the olanzapine $[M+H]^+$ peak in each pixel within the selected clusters are divided by the respected cluster specific TEC shown in figure 2D. The mean normalised intensities are now aligned across clusters, with regional differences largely eliminated. No significant difference in normalised intensity is observed between the selected clusters for either DESI or MALDI data (ANOVA, $p>0.1$). Figure 2F shows an image of the normalised intensity of olanzapine $[M+H]^+$ using TECs calculated for all 15 clusters as regional normalisation factors. In comparison to the unnormalised image shown in figure 2A, intensity appears notably more homogenous, with the visibility and contrast of anatomical features considerably reduced by the application of TEC based normalisation.

Concentration dependence of analyte suppression in MALDI MSI

To explore the impact of concentration on levels of analyte suppression, horizontal mouse brain sections were sprayed with 0.1, 0.5 or 1 mg/ml olanzapine, resulting in calculated olanzapine densities of 0, 77, 384 and 767 pmol/mm^2 respectively. CHCA matrix was subsequently applied and MALDI MSI performed at a nominal pixel size of 45 µm. Graph cuts clustering was applied separately to datasets from each olanzapine density. When clustered with k=17, ten distinct anatomical regions were able to be matched across the four samples. In reference to a horizontal mouse brain atlas these were tentatively identified as (1) the fimbria and genu of the corpus callosum, (2) the corpus callosum, (3) arbour vitae (white matter of the cerebellum), (4) superior colliculus, (5) striatum, (6) deeper layers of the cerebral cortex, (7) periaqueductal grey matter, (8) granular layer of the cerebellum, (9) hippocampus and (9) the molecular layer of the cerebellum (ranked from highest to lowest cluster-specific TEC at 768 pmol/mm^2 as shown in figure 3). The remaining seven clusters were not able to be matched across graph cuts segmentation performed on each section.

For each cluster, TECs were calculated from the mean intensity of olanzapine in the cluster ROI and the mean olanzapine intensity of the off-tissue region for the respective concentration. Boxplots of cluster intensity are shown in figure S-2. The concentration dependence of cluster specific TECs for the 10 matched clusters is compared in figure 3. A clear separation is observed between three clusters identifiable as white matter regions, and the remaining clusters, identifies as various grey matter regions. White matter clusters show a strong positive correlation between cluster-specific TEC and olanzapine concentration ($R^2 > 0.95$), while grey matter clusters do not appear to follow the same trend ($R^2< 0.3$). At the highest concentration of olanzapine the lowest TEC for a white matter cluster (0.104 for the arbour vitae) is over twice that of the highest TEC for a grey matter cluster (0.045,colliculus). For

white matter clusters, the relationship between analyte concentration and TEC appears to be somewhat non-linear, and may have an exponential component, although further data points would be required to confirm. For grey matter clusters, the TEC increases at low concentrations before plateauing or dropping at the higher concentrations. For the molecular layer of the cerebellum, the TEC is observed to drop with increasing olanzapine concentration. These very different behaviours reflect the complex environments from which the matrix effects driving analyte suppression arise.

The concentration dependence of regionally specific suppression effects is particularly important to understand for those considering quantitative mass spectrometry imaging in complex tissues. Different approaches for placing calibration standard curves for quantitative MSI have been reported, including deposition across regions of heterogeneous anatomy[43–45], or a deposition in a single anatomical region[25]. Unless appropriate normalisation strategies are implemented, spatial differences in ion suppression may disrupt both the linearity of the calibration curve and accurate quantitation across regions of distinct TEC. This could result significant discrepancies between calculated and actual analyte concentrations if a calibration curve generated on a low-TEC regions was used without normalisation to predict analyte concentration in a high-TEC region. For example, if olanzapine in the white matter of an *in vivo* dosed animal was quantified by MALDI MSI, using a calibration curve spotted on a large grey matter region such as the cerebral cortex, the concentration calculated without appropriate normalisation could be over 5 times higher than the actual concentration in the sample due to the reduced ion suppression observed between the two regions.

Comparing cluster-specific TEC normalisation to other methods

The most commonly used normalisation methods in MSI operate in an unsupervised pixel-wise approach. We compared the effectiveness of 6 normalisation methods made available in Spectral Analysis software[24] to normalise the intensity of olanzapine in the DESI and MALDI MSI datasets. Normalised images of the olanzapine $[M+H]^+$ peak are shown in figure 4. An effectively normalised image would present a homogenous intensity of olanzapine across the image. In many of the normalised images, anatomical features remain visible. The olanzapine images normalised by the median intensity, noise level or TIC appear little different compared to the unnormalised image (figure 4, far left) for both DESI and MALDI. After L2 and RMS normalisation, contrast between white and grey matter regions are reduced although, anatomical features including the white matter and hippocampus remain visible. P-norm normalisation appears to produce the most even normalised olanzapine intensity across tissue

regions for MALDI, but appears similar in effectiveness to RMS and L2 normalisation for the DESI dataset. While all data presented was obtained on an Q-ToF mass analyser, expected noise levels will differ between ToF, Q-ToF and FT mass analysers [20]. Analyser type should therefore be considered when selecting an appropriate normalisation methods.

Normalisation of olanzapine by cluster specific TECs is shown in figure 4 for 15 and 50 clusters. With 15 clusters used for TEC normalisation, olanzapine intensity appears to be more noticeably more homogenous than any of the six pixel-wise approaches shown alongside. Some anatomical features, such as the white matter for the MALDI dataset and layers of the cerebral cortex for the DESI dataset, remain faintly visible, although their relative contrast is noticeably reduced compared to other considered normalisation methods. At 15 clusters many of the major anatomical regions expected at this level and plane of the mouse brain are segmented. However, we hypothesised that increasing the number of clusters segmented would result in more effective normalisation. At 50 clusters segmentation appears effective with clusters visually correlating to expected anatomical regions (Figure S-3). Normalising by cluster-specific TECs from these 50 clusters results in a noticeably more effective normalisation for both MALDI and DESI datasets, with the visibility of anatomical features in the olanzapine intensity reduced. With further increases in cluster number to 500, little or no improvement in normalisation effectiveness is observed, and additional clusters do not correspond to expected anatomical features but are rather speckled across the tissue. (Figure S-3). Normalisation effectiveness at increasing cluster numbers can be assessed by the RSD of the normalised image (Figure S-4). For the DESI dataset high cluster numbers RSD appears to increase following a minima at ~k=50, highlighting the potential for over-clustering. For many segmentation methods, selecting the number of segments or clusters is a subjective choice for the user. Here the RSD of a cluster-specific TEC normalised image of a homogeneous analyte may be used as a surrogate to select cluster number.

In its application to date, TECs have been calculated from the mean intensity of the analyte in the on- and off-tissue regions. However, where a “hot spot” or “dead pixel” is present, this may lead to a non-normal distribution of intensities. If the mean is not an appropriate statistical representation of the intensity distribution, the calculated TEC may not best reflect suppression in that region. Future applications of such approaches should consider the most appropriate summary statistic, possibly the median intensity, to provide robust normalisation that is less susceptible to the influence of “hot” or “dead” pixels .Similarly, where regions of interest boarder the edge of the tissue, accurate segmentation

of the tissue from the background is essential to avoid the influence of any "halo" on summary statistics from the region of interest. Here, tissue was effectively segmented from background using *k*-means (k=2, cosine distance).

Spectral differences between anatomical regions identified in DESI and MALDI MSI

To date, few studies have compared the information obtained from MALDI and DESI data from the same sample type. We recognised the opportunity to compare mean spectra from matched clusters from the data presented in this paper. Figure 5A shows mean spectra between m/z 400-1200 from the four matched clusters from DESI and MALDI MSI discussed earlier. Mean spectra for all clusters from DESI and MALDI MSI are provided in figures S-4 & S-5. From a subtraction of these mean spectra, several prominent peaks more prevalent in each technique were identified and tentatively assigned (Table 2). Notable peaks specific to DESI data include include some phosphatidylcholines seen all clusters, and others more prominently seen in specific cluster. Notable peaks specific to MALDI data include members of phosphatidylcholine, phosphatidic acid and phosphatidylglycerol lipid classes.

To compare the number of distinct species identified in DESI and MALDI MSI from the same clusters, peaks from mean spectra were matched against the HMDB database. Figure 5B show venn diagrams for each matched cluster. Most notable is the relatively small overlap of species observed in both DESI and MALDI for all clusters. The majority of identified species (mean of 85% for all four matched clusters) are uniquely observed by one technique only, indicating the importance of multi-technique studies to provide wide species coverage. Comparing between techniques for the same matched clusters, 3.5 times more species are uniquely identified from DESI data than from MALDI data (Mean. Range = 0.74-6.00 times). This demonstrates the power of database matching of spectra from segmented regions to compare the relative chemical information provided by complementary ionisation methods in the context of assessing ion suppression, and will be further explored in future studies.

Conclusions

In this study we have explored aspects of regionally specific ion suppression in DESI and MALDI mass spectrometry imaging. Calculation of TECs for multiple anatomical regions, identified by graph-cuts clustering, enabled clear comparison of different relative ion suppression effects in heterogeneous tissues, extending the approach first proposed by Hamm *et al.* for whole body sections. While significant differences in relative ion suppression was seen between grey and white matter associated clusters for both techniques, this was most stark in MALDI MSI. Further exploration of ion suppression in MALDI revealed a strong concentration dependence on ion suppression in white matter clusters. These investigations help reveal the complexity of ion suppression in multiple MSI modalities and the challenges in interpreting data from heterogeneous tissues. Future studies on ion suppression should also consider structural as well as chemical differences between regions exhibiting different ion suppression behaviours. Possible structural characteristics of interest include cell density[46–48], nuclei density and overall tissue density[49]. While no clear differences in the distribution of sodium and potassium adducts of the same species were observed, the distribution of endogenous salts will also be important to consider in future studies.

Graph cuts clustering enabled the clear segmentation of anatomical regions that could be matched across datasets. The development of routines for automated matching of clusters across sections and across techniques would prove useful in a number of cases. A current challenge for segmentation methods is the selection of appropriate cluster number. Further work to develop metrics to assess this would be useful. We have also demonstrated the potential to use custer-specific TECs as regional normalisation factors. Future work here should explore the potential to apply regional-TECs calculated from one section to sections from other animals; conceivably enabling predictive normalisation of *in vivo dosed* samples.

Few studies to date have considered DESI and MALDI analysis of the same sample. While similar samples have been studied here, a number of differences, including the exact section depth, as well as the olanzapine coating, prevent a full review of analytes detected by each technique, and in each anatomical region. This work, however, provides methods and workflows for a more complete comparison between

these techniques, as well as for intra-technique variables such as polarity, MALDI matrix, and DESI solvent system.

Supporting information

Supporting information is provided including plots further detailing concentration dependent ion suppression in MALDI MSI, selection of cluster number, and mean spectra from all clusters for comparison of DESI and MALDI MSI.

References

(1) Guilbault, G. G.; Hjelm, M. *J. Macromol. Sci. Part A Pure Appl. Chem.* **1989**, *61*, 1657–1664.
(2) Dong, Y.; Guella, G.; Franceschi, P. *Rapid Commun. Mass Spectrom.* **2016**, *30*, 711–718.
(3) Muramoto, S.; Forbes, T. P.; van Asten, A. C.; Gillen, G. *Anal. Chem.* **2015**, *87*, 5444–5450.
(4) Steven, R. T.; Dexter, A.; Bunch, J. *Methods* **2016**, *104*, 111–117.
(5) Steven, R. T.; Race, A. M.; Bunch, J. *J. Am. Soc. Mass Spectrom.* **2016**, *27*, 1419–1428.
(6) Steven, R. T.; Dexter, A.; Bunch, J. *Methods* **2016**, *104*, 101–110.
(7) Hamm, G.; Bonnel, D.; Legouffe, R.; Pamelard, F.; Delbos, J.-M.; Bouzom, F.; Stauber, J. *J. Proteomics* **2012**, *75*, 4952–4961.
(8) Hankin, J. A.; Murphy, R. C. *Anal. Chem.* **2010**, *82*, 8476–8484.
(9) Fonville, J. M.; Carter, C.; Cloarec, O.; Nicholson, J. K.; Lindon, J. C.; Bunch, J.; Holmes, E. *Anal. Chem.* **2012**, *84*, 1310–1319.
(10) Ifa, D. R.; Manicke, N. E.; Rusine, A. L.; Cooks, R. G. *Rapid Commun. Mass Spectrom.* **2008**, *22*, 503–510.
(11) Shard, A. G.; Spencer, S. J.; Smith, S. A.; Havelund, R.; Gilmore, I. S. *Int. J. Mass Spectrom.* **2015**, *377*, 599–609.
(12) Jones, E. A.; Lockyer, N. P.; Kordys, J.; Vickerman, J. C. *J. Am. Soc. Mass Spectrom.* **2007**, *18*, 1559–1567.
(13) Jones, E. A.; Lockyer, N. P.; Vickerman, J. C. *Int. J. Mass Spectrom.* **2007**, *260*, 146–157.
(14) Jones, E. A.; Lockyer, N. P.; Vickerman, J. C. *Appl. Surf. Sci.* **2006**, *252*, 6727–6730.
(15) Vorng, J.-L.; Kotowska, A. M.; Passarelli, M. K.; West, A.; Marshall, P. S.; Havelund, R.; Seah, M. P.; Dollery, C. T.; Rakowska, P. D.; Gilmore, I. S. *Anal. Chem.* **2016**, *88*, 11028–11036.
(16) Lanekoff, I.; Stevens, S. L.; Stenzel-Poore, M. P.; Laskin, J. *Analyst* **2014**, *139*, 3528–3532.
(17) Frick, D. A.; Giesen, C.; Hemmerle, T.; Bodenmiller, B.; Günther, D. *J. Anal. At. Spectrom.* **2015**, *30*, 254–259.
(18) Swales, J. G.; Strittmatter, N.; Tucker, J. W.; Clench, M. R.; Webborn, P. J. H.; Goodwin, R. J. A. *Sci. Rep.* **2016**, *6*, 37648.
(19) Kertesz, V.; Vavrek, M.; Freddo, C.; Van Berkel, G. J.; Cahill, J. F.; Weiskittel, T. M. *Anal. Chem.* **2016**, *88*, 6026–6034.
(20) Deininger, S.-O.; Cornett, D. S.; Paape, R.; Becker, M.; Pineau, C.; Rauser, S.; Walch, A.; Wolski, E. *Anal. Bioanal. Chem.* **2011**, *401*, 167–181.
(21) Bergman, H.-M.; Lundin, E.; Andersson, M.; Lanekoff, I. *Analyst* **2016**, *141*, 3686–3695.
(22) Griffiths, R. L.; Bunch, J. *Rapid Commun. Mass Spectrom.* **2012**, *26*, 1557–1566.
(23) Griffiths, R. L.; Sarsby, J.; Guggenheim, E. J.; Race, A. M.; Steven, R. T.; Fear, J.; Lalor, P. F.; Bunch, J. *Anal. Chem.* **2013**, *85*, 7146–7153.
(24) Race, A. M.; Palmer, A. D.; Dexter, A. J.; Steven, R. T.; Styles, I. B.; Bunch, J. *Anal. Chem.* **2016**, *88*, 9451–9458.
(25) Källback, P.; Nilsson, A.; Shariatgorji, M.; Andrén, P. E. *Anal. Chem.* **2016**, *88*, 4346–4353.
(26) Källback, P.; Shariatgorji, M.; Nilsson, A.; Andrén, P. E. *J. Proteomics* **2012**, *75*, 4941–4951.
(27) Stoeckli, M.; Staab, D.; Schweitzer, A. *Int. J. Mass Spectrom.* **2007**, *260*, 195–202.
(28) Pirman, D. A.; Kiss, A.; Heeren, R. M. A.; Yost, R. A. *Anal. Chem.* **2013**, *85*, 1090–1096.
(29) Hansen, H. T.; Janfelt, C. *Anal. Chem.* **2016**, *88*, 11513–11520.
(30) Kompauer, M.; Heiles, S.; Spengler, B. *Nat. Methods* **2017**, *14*, 90–96.
(31) Dexter, A.; Race, A. M.; Styles, I. B.; Bunch, J. *Anal. Chem.* **2016**, *88*, 10893–10899.
(32) Dexter, A.; Race, A. M.; Steven, R. T.; Barnes, J. R.; Hulme, H.; Goodwin, R. J. A.; Styles, I. B.; Bunch, J. *Anal. Chem.* **2017**, *89*, 11293–11300.

(33) Schramm, T.; Hester, A.; Klinkert, I.; Both, J.-P.; Heeren, R. M. A.; Brunelle, A.; Laprévote, O.; Desbenoit, N.; Robbe, M.-F.; Stoeckli, M.; Others. *J. Proteomics* **2012**, *75*, 5106–5110.
(34) Race, A. M.; Styles, I. B.; Bunch, J. *J. Proteomics* **2012**, *75*, 5111–5112.
(35) R Core Team. *R: A Language and Environment for Statistical Computing*; R Foundation for Statistical Computing: Vienna, Austria, 2013.
(36) Race, A. M.; Bunch, J. *Anal. Bioanal. Chem.* **2015**, *407*, 2047–2054.
(37) Garnier, S. Viridis: Default Color Maps from "matplotlib" https://CRAN.R-project.org/package=viridis (accessed Dec 1, 2017).
(38) matplotlib colormaps https://bids.github.io/colormap/ (accessed Dec 1, 2017).
(39) Wishart, D. S.; Tzur, D.; Knox, C.; Eisner, R.; Guo, A. C.; Young, N.; Cheng, D.; Jewell, K.; Arndt, D.; Sawhney, S.; Fung, C.; Nikolai, L.; Lewis, M.; Coutouly, M.-A.; Forsythe, I.; Tang, P.; Shrivastava, S.; Jeroncic, K.; Stothard, P.; Amegbey, G.; Block, D.; Hau, D. D.; Wagner, J.; Miniaci, J.; Clements, M.; Gebremedhin, M.; Guo, N.; Zhang, Y.; Duggan, G. E.; Macinnis, G. D.; Weljie, A. M.; Dowlatabadi, R.; Bamforth, F.; Clive, D.; Greiner, R.; Li, L.; Marrie, T.; Sykes, B. D.; Vogel, H. J.; Querengesser, L. *Nucleic Acids Res.* **2007**, *35*, D521–D526.
(40) Wishart, D. S.; Knox, C.; Guo, A. C.; Eisner, R.; Young, N.; Gautam, B.; Hau, D. D.; Psychogios, N.; Dong, E.; Bouatra, S.; Mandal, R.; Sinelnikov, I.; Xia, J.; Jia, L.; Cruz, J. A.; Lim, E.; Sobsey, C. A.; Shrivastava, S.; Huang, P.; Liu, P.; Fang, L.; Peng, J.; Fradette, R.; Cheng, D.; Tzur, D.; Clements, M.; Lewis, A.; De Souza, A.; Zuniga, A.; Dawe, M.; Xiong, Y.; Clive, D.; Greiner, R.; Nazyrova, A.; Shaykhutdinov, R.; Li, L.; Vogel, H. J.; Forsythe, I. *Nucleic Acids Res.* **2009**, *37*, D603–D610.
(41) Wishart, D. S.; Jewison, T.; Guo, A. C.; Wilson, M.; Knox, C.; Liu, Y.; Djoumbou, Y.; Mandal, R.; Aziat, F.; Dong, E.; Bouatra, S.; Sinelnikov, I.; Arndt, D.; Xia, J.; Liu, P.; Yallou, F.; Bjorndahl, T.; Perez-Pineiro, R.; Eisner, R.; Allen, F.; Neveu, V.; Greiner, R.; Scalbert, A. *Nucleic Acids Res.* **2013**, *41*, D801–D807.
(42) Rosen, G. D.; Williams, A. G.; Capra, J. A.; Connolly, M. T.; Cruz, B.; Lu, L.; Airey, D. C.; Kulkarni, K.; Williams, R. W. In *Int Mouse Genome Conference*; 2000; p 14:166.
(43) Shariatgorji, M.; Nilsson, A.; Goodwin, R. J. A.; Källback, P.; Schintu, N.; Zhang, X.; Crossman, A. R.; Bezard, E.; Svenningsson, P.; Andren, P. E. *Neuron* **2014**, *84*, 697–707.
(44) Shariatgorji, M.; Strittmatter, N.; Nilsson, A.; Källback, P.; Alvarsson, A.; Zhang, X.; Vallianatou, T.; Svenningsson, P.; Goodwin, R. J. A.; Andren, P. E. *Neuroimage* **2016**, *136*, 129–138.
(45) Pirman, D. A.; Reich, R. F.; Kiss, A.; Heeren, R. M. A.; Yost, R. A. *Anal. Chem.* **2013**, *85*, 1081–1089.
(46) Herculano-Houzel, S.; Mota, B.; Lent, R. *Proc. Natl. Acad. Sci. U. S. A.* **2006**, *103*, 12138–12143.
(47) Herculano-Houzel, S.; Lent, R. *J. Neurosci.* **2005**, *25*, 2518–2521.
(48) Herculano-Houzel, S.; Watson, C.; Paxinos, G. *Front. Neuroanat.* **2013**, *7*, 35.
(49) Bilkey, J.; Tata, A.; McKee, T. D.; Porcari, A. M.; Bluemke, E.; Woolman, M.; Ventura, M.; Eberlin, M. N.; Zarrine-Afsar, A. *Anal. Chem.* **2016**, *88*, 12099–12107.

Figures for

“Exploring Ion Suppression in Mass Spectrometry Imaging of a Heterogeneous Tissue”

Adam J Taylor (1)
Alex Dexter (1)
Josephine Bunch* (1,2)

1. National Centre of Excellence in Mass Spectrometry Imaging (NiCE-MSI), National Physical Laboratory, Hampton Road, Teddington, TW11 0LW, UK
2. Department of Surgery and Cancer, Imperial College London, South Kensington Campus, London, SW7 2AZ, UK

* Corresponding author. Email: josephine.bunch@npl.co.uk

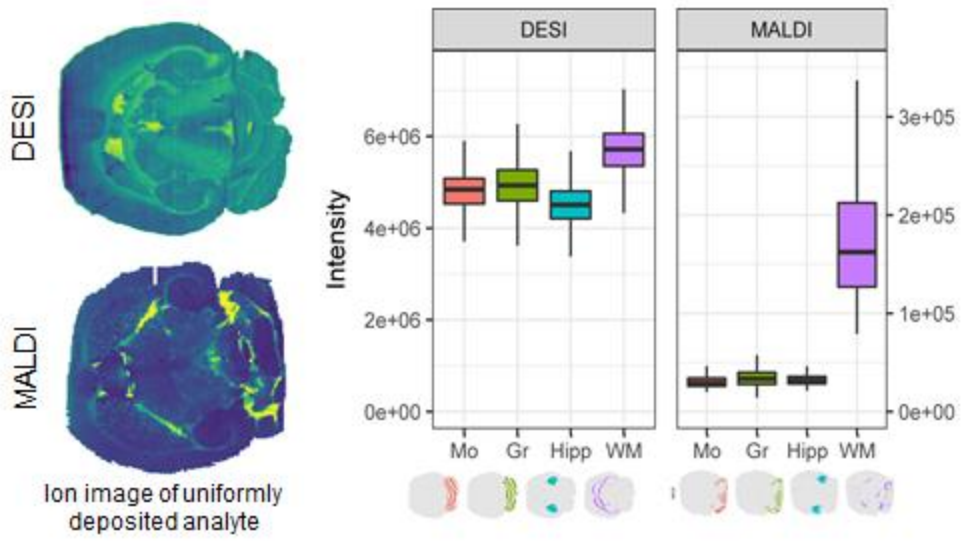

Table of contents graphic

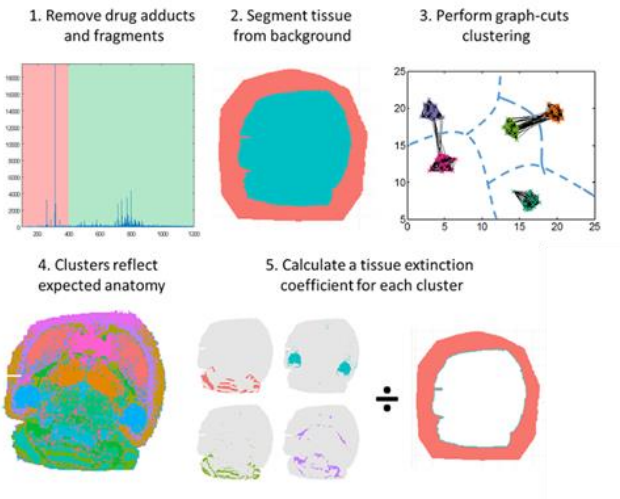

Figure 1. Data processing workflow for calculation of cluster-specific TECs

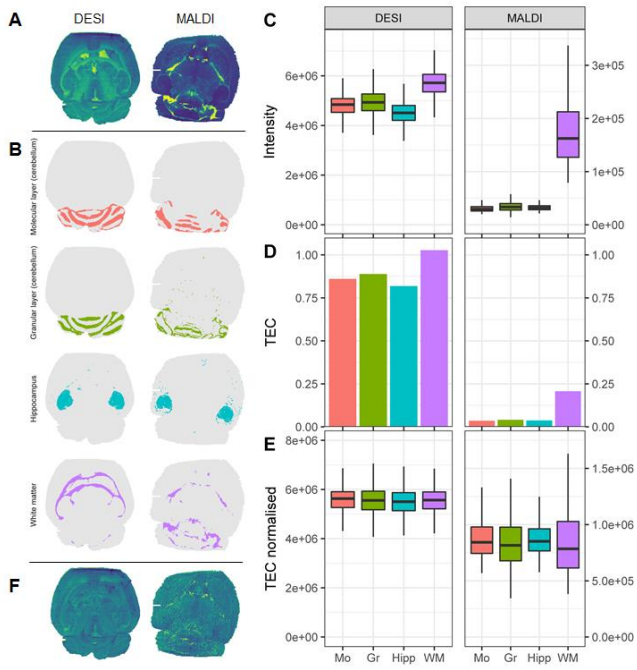

Figure 2. *Comparing suppression of Olanzapine in DESI and MALDI MSI. Olanzapine was homogeneously deposited by sublimation on 10 µm horizontal cryosections of whole mouse brain, and analysed by DESI and MALDI MSI. (A) DESI (left) and MALDI (right) MSI images of Olanzapine $[M+H]^+$ (m/z 313.14). (B) Selected matched clusters from graph-cuts clustering (k=15) of DESI (left) and MALDI (right) MSI data, corresponding (top to bottom) to the molecular (Mo) and granular (Gr) layers of the cerebellum, hippocampus (Hipp) and white matter (WM). Images are not shown to scale. (C) Boxplots of Olanzapine $[M+H]^+$ intensity in each selected cluster. (D) Calculated tissue extinction coefficients for selected clusters. (E) Boxplots of TEC normalised Olanzapine [M+H]+ intensity for each cluster. Boxplots show median (bar), first and third quartiles (box) and the largest and smallest values no further than 1.5 × IQR (whiskers). (F) DESI (left) and MALDI (right) MSI images of Olanzapine [M+H]+ after normalisation by cluster-specific TECs. MSI images and clusters are not shown to scale relative to one another.*

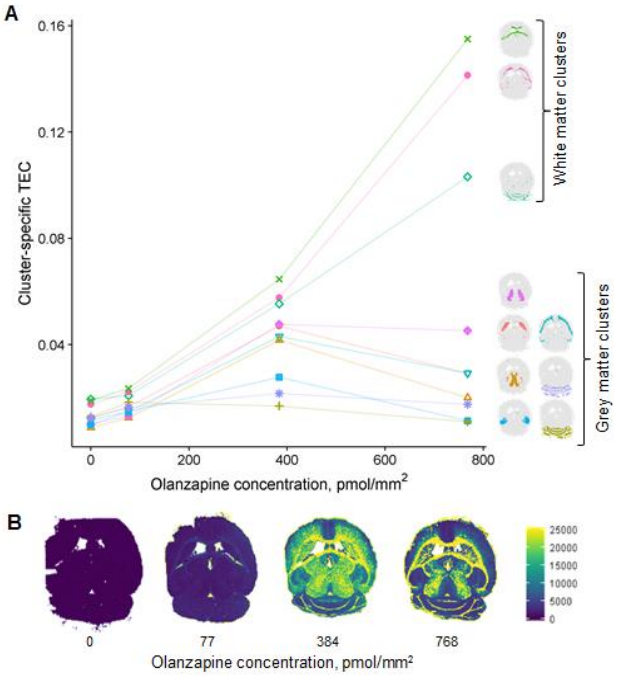

Figure 3. *(A) plot showing concentration dependence of cluster-specific TECs. Cluster images, are shown on the right. Colour is required to interpret this plot. (B) Single ion images of Olanzapine $[M+H]^+$ (m/z 313.15), deposited by spraying, at 0, 77, 384 and 768 pmol/mm^2 calculated Olanzapine density.*

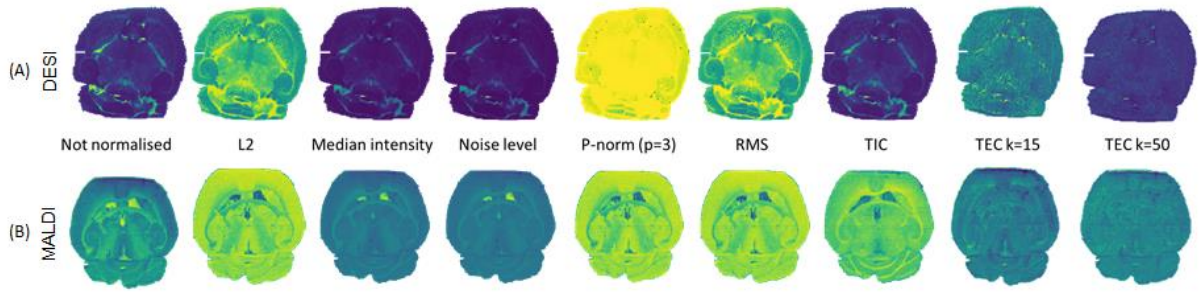

Figure 4. Published normalisation methods and TEC normalisation applied to (A, top) DESI and (B, bottom) MALDI MSI of sublimed Olanzapine on mouse brain. Normalisation methods (left-to-right): Not normalised, L2 normalisation, median intensity normalisation, noise level normalisation, P-norm normalisation (p=3), root mean square (RMS) normalisation, total ion count (TIC) normalisation and TEC normalisation (k=15 and k=50).

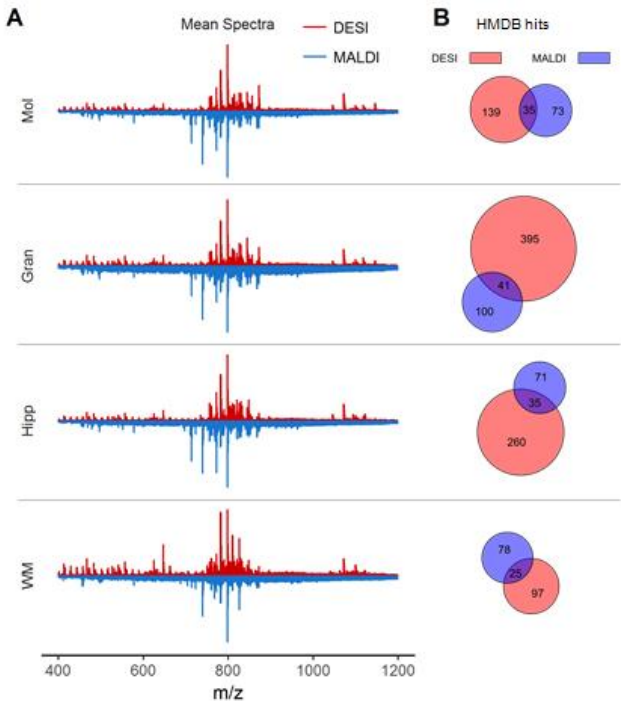

Figure 5. (A) Mean spectra from selected matched clusters (Top to bottom: Molecular and granular regions of the cerebellum, hippocampus, white matter) from DESI (red) and MALDI (blue, inverted) MSI. Intensity scale is consistent across clusters from the same MSI technique. Mean spectra for all regions are shown in figures S-5 (DESI) and S-6 (MALDI). (B) Venn diagrams showing number of hits identified from the HMDB database for matched clusters in DESI (red) and MALDI (blue). Circle area is proportional to number. Venn diagrams are scaled to enable comparison across clusters. Potential hits were filtered by mass accuracy (<10 ppm) and ^{13}C isotope image correlation.

	Tissue extinction coefficient (TEC)	
Region	DESI	MALDI
Molecular layer (cerebellum)	0.860	0.035
Granular layer (cerebellum)	0.888	0.041
Hippocampus	0.891	0.037
White matter	1.027	0.207

Table 1. Tissue extinction coefficients for olanzapine for selected matched regions from DESI and MALDI datasets shown in figure 2.

Observed m/z	**Potential assignments**	**Prevalent technique**	**Prevalent region**
782.57	PC(36:4) $[M+H]^+$ PC(34:1) $[M+Na]^+$	DESI	All
810.60	PC(38:4) $[M+H]^+$ PC(36:1) $[M+Na]^+$	DESI	WM
1072.72	PC(34:1)-isoLG lactam $[M+Na]^+$ MIPC(42:0)	DESI	All
872.55	LacCer(32:1) $[M+K]^+$ PC(40:6) $[M+K]^+$	DESI	Mol
828.56	PC(40:9) $[M+H]^+$ PC(38:6) $[M+Na]^+$	DESI	Gran
739.46	PG(34:6) $[M+H]^+$ PC(34:1) $[M-N(CH_3)_3+K]^+$	MALDI	All
713.45	PA(34:1) $[M+K]^+$ PC(32:0) $[M-N(CH_3)_3+K]^+$	MALDI	Not WM
772.52	PC(32:0) $[M+K]^+$	MALDI	Mol & Hip

Table 2. Notable peaks and their tentative assignments differentiating between MALDI and DESI MSI mean spectra for matched regions shown in figure 5A.